

3D measurement of tool wear with the in-process image based on a new auto-regressive calibration algorithm in ultra-precision raster milling

S.J. Zhang¹, S. To^{1#}, C.F. Cheung¹ and J.J. Du²

¹ State Key Laboratory in Ultra-precision Machining Technology, Department of Industrial and Systems Engineering, The Hong Kong Polytechnic University, Hung Hom, Kowloon, Hong Kong SAR, China.

² Shenzhen Graduate School, Harbin Institute of Technology, Shenzhen, PR China

Corresponding Author / E-mail: mfsto@inet.polyu.edu.hk, TEL: +852-2766-6587, FAX: +852-2764-7657

KEYWORDS : tool wear, in-process, 3D measurement, auto-regressive calibration, ultra-precision raster milling

In this paper, a new auto-regressive calibration algorithm is proposed to reconstruct 3D topographic surface of a single crystal diamond tool wear based on its in-process image and is embedded into an in-process measurement system mounted on an ultra-precision raster milling machine in order to monitor tool wear condition. That is because the slight tool wear will influence the surface quality of work-piece due to the long machining time for high precision optical surface in the ultra-precision raster milling. Preliminarily, based on principle digital image processing technique such as median filtering, threshold segmentation, edge detection and Hough arc transform, tool wear lands are separated from a tool wear image captured by a CCD camera with one 100X lens and the influence of disturbance such as cutting fluid and chipping in un-wear lands is avoided; Secondly, a traverse search method of arc translation is put forward to eliminate feigned wear lands, and then a least square polynomial method is adopted to fit the inner- and outer-contours of wear lands, which can self-adaptively eliminate the influence of high frequency noises on tool wear lands and connect the discontinuous wear lands; Finally, the auto-regressive calibration method is used to reconstruct its 3D topographic wear surface which is compared with its photograph taken by scan electron microscopy (SEM). In a word, the wear surface can be extracted self-adaptively, and the wear area, maximal tool wear width and average tool wear width and worn volume are calculated automatically by the algorithm. The result indicates the method provides a possibility for its in-process 3D-wear measurement in ultra-precision raster milling and the algorithm reliability is validated finally.

Manuscript received: January XX, 2011 / Accepted: January XX, 2011

NOMENCLATURE

VB = the average wear width

VB_{max} = the maximal wear width

x = row coordinate of image

y = column coordinate of image

g = segmented image

f = grey level

T_0, T_1, \dots, T_k = a series of thresholds

$k = 1, 2, \dots, 255$

n_1 = a given refractive index

n_2 = a second medium with refractive index

R = the reflection coefficient

θ_i = refraction angle of light

θ_i' = incident angle of light

of high precision and high quality in machining non-rotational symmetric freeform surfaces with nano-metric surface roughness and sub-micrometric form error. In long-time milling processes, the SCDT wear in such a nanometer condition is significant as slight degradation of tool will lead to poor surface quality of extremely high precision components in UPRM. And in UPRM, the time required for setting up is much longer than in conventional machining. More importantly, the machining time is generally several weeks, or even a month long in the manufacture of freeform products. If tool failure occurs, the previous setup time and the previous machining time will be wasted so that it lowers productivity and induces a huge economic loss. In order to improve components' quality and productivity, in-process or on-line measurement of tool wear is very extremely important and essential for UPRM.

Tool wear affects surface roughness and dimensional accuracy. Many researchers have used various sensors, acoustic emission (AE) [1], dynamometers [2], vibration [3], ultrasonic vibrations [4], and motor spindle speed and power consumption [5] to monitor drill wear. The relationship was established between force signals and flank

1. Introduction

Ultra-precision raster milling (UPRM) with a single crystal diamond tool (SCDT) is widely used to produce optical components

wear under other cutting parameters when drilling a copper alloy [6]. The vibration signal processing [7] and investigation between tool wear and cutting force [8] have been analyzed for tool wear detection. The optical methods were essentially off-line and involved the examination of geometry using a specially adapted toolmaker's microscope for the digital processing of the tool tip image [5, 9-16]. The relationship between tool wear and surface roughness was discussed [17, 18]. Various researchers have applied them to measure flank wear and crater wear (11-13, 21-23). Various studies on tool wear in single point diamond turning or conventional machining have been conducted by researchers, but little attention has been paid to in-process or on-line monitoring the SCDT wear in UPRM.

However, nowadays in UPRM, the workers only make use of their experience to decide whether a tool is replaced by a new one or not, so, when tool wear happens slightly but not heavily enough to influence surface quality of high precision components, the setting-up time is wasted so that the machining-down time is increased and the productivity is lowered, or when tool wear has been so great, if the tool wear is not detected, it weakens surface quality. In this study, firstly, an in-process measurement system is built up with a CCD camera and one piece of 100X microscopy lens is implemented on the Precitech Freeform Machine 705G to acquire a tool wear image. Secondly, a new auto-regressive calibration algorithm, where 3D topography of tool wear lands is reconstructed, based on the in-process image of tool wear by employing digital signal processing technique, to extract tool wear features, is developed. Finally, the 3D topography of tool wear reconstructed by using the auto-regressive calibration algorithm is compared with the tool photograph of scan electron microscopy (SEM) employed to observe its wear surface features. In a word, surface topography of tool wear is extracted self-adaptively and the algorithm calculates tool wear features such as the wear area, maximal wear width, average wear width and wear volume automatically. The reliability of algorithm is identified.

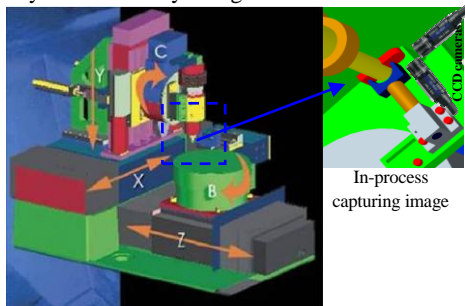


Fig.1 Schematic configuration of a UPRM machine and an in-process 3D measurement system

2. Experimental Set-up and Results

2.1 Experimental Set-up

In Fig.1, schematic configuration of a UPRM machine (Precitech 705G) is shown. The UPRM machine possesses three linear axes (X, Y and Z) and two rotational axes (B and C), a single crystal diamond tool (SCDT) is set up on the spindle and the workpiece is installed on the B axis rotation table.

An in-process measurement system of tool wear is mounted in the machine of Precitech 705G, which includes a CCD camera with one piece of 100X microscopy lens positioned on B-axis as schematically shown in Fig.1. Before an image of rake face of a SCDT is captured, the tool must be cleared through pressure-air, and then influence of some of a little coolant and chips still remaining are removed from the image by digital image processing technique. The tool parameters

are shown in Tab.1, which are used to calibration image pixels.

Tab.1 SCDT parameters

Cutting edge radius	0.001(μm)
Tool rake angle	0°
Tool (nose) radius	0.017 mm
Front clearance angle	15°

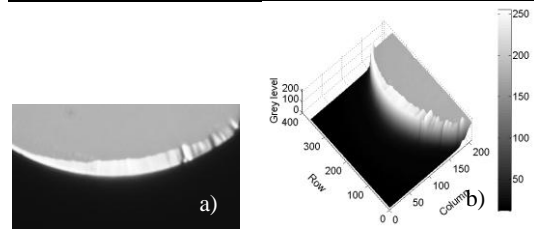


Fig.2 Rake face image of a SCDT after wear a) its optical image (100X) and b) its 3D grey image

2.2 Digital Image Processing Technique

From the SCDT image captured by the CCD camera with a 100X lens in the normal direction of the tool rake face, as shown in Fig.2a), it is known that the background (black), un-wear land (grey) and wear land (white) are at different grey levels which provide the thresholds of separating the wear land from the un-wear land and background.

The tool wear lands (white) are composed of outer- and inner-contours, and Fig.2b shows a 3-D grey level image. From the image, the grey levels of three regions are extremely distinctly different, the grey gradient from three different regions changes abruptly with harmful effects of coolant remains, chips and light.

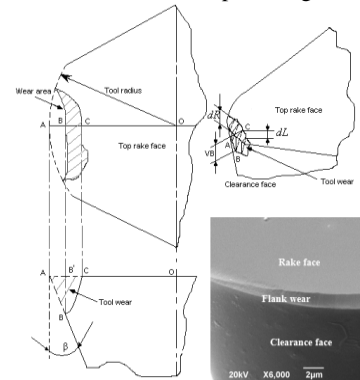


Fig.3 Schematic illustration of tool wear characterization

The schematic illustration of tool wear characterization is outlined as shown in Fig.3, where the β is the front clearance angle of a SCDT, A-curve is the arc of tool nose, B' or B-curve is the outer-contour of tool wear and C-curve is the inner-contour of tool wear. Moreover, BC-curve is constituted as the tool wear surface or profile. AC-land is a worn land, and BC-land is a wear land, respectively.

As mentioned above, the problems which need to be solved include eliminating the feigned wear lands (white) in the un-wear land, smoothing and continuing the wear lands, removing the noise, and finally, 3D-reconstructing topographic surface of the tool wear lands. Preliminarily, based on digital image pre-processing technique such as averaging filter, threshold segmentation, edge detection and Hough arc transform of tool nose, it is a key to efficiently separate wear lands from the image to avoid influence of disturbance such as coolant remains and chips. Secondly, after the digital image pre-processing method, a traverse search method of arc translation is put forward to eliminate feigned wear lands, and then a least square polynomial method is adopted to fit inner- and outer-contours of wear lands, which self-adaptively eliminates influence of high frequency

(HF) noise and connects discontinuous wear lands. Finally, a new auto-regressive calibration algorithm is developed to derive BC-curve of tool wear lands separated by previous methods to reconstruct 3D topography of tool wear lands and to obtain tool wear features. To identify the method, SEM is employed to view its photograph. The flow chart of the 3D measurement method of tool wear based on the in-process image is shown in Fig.4.

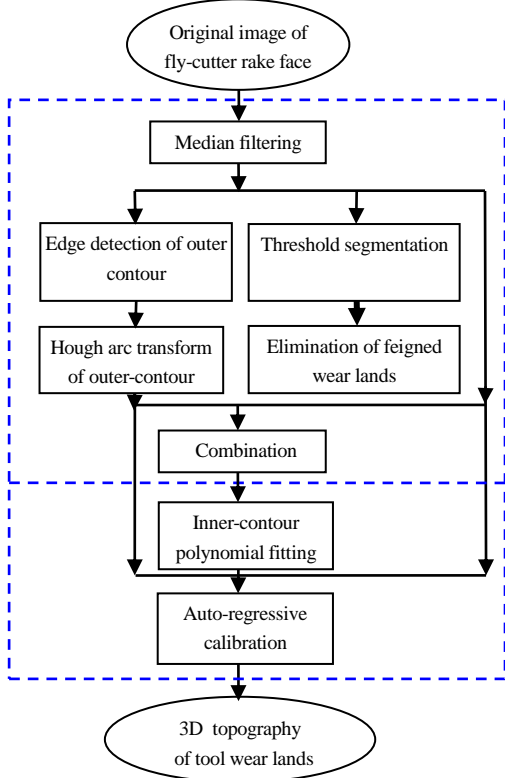


Fig.4 Flow chart of the algorithm

2.2.1 Threshold Segmentation

Threshold segmentation is relatively a simple approach to segment an image into regions of similarity. The basic principle is to group pixels within a common range of grey levels into a pre-determined set, which is defined by

$$g(x, y) = k \quad (T_{k-1} \leq f(x, y) < T_k, \quad k = 1, 2, \dots, 255), \quad (1)$$

By the grey-level histogram of the initial tool wear image (Fig.2a), as shown in Fig.5, two thresholds are the values of two wave troughs in its histogram. The two thresholds are set to segment the image $A(x, y)$ (Fig.2a) to obtain a new one for which the grey values are only three grey values (tri-values), the background of the image (back) 0, the un-wear land (grey) 127, and the wear land (white) 255. The new image is denoted as $B(x, y)$, as shown in Fig.6.

2.2.2 Edge Detection and Hough Arc Transform

The Sobel edge detector is an extension which includes a degree of smoothing to automatically reduce certain artifacts caused by noise. The larger the filter array, the more noise reduction occurs with fewer edges being extracted, but as the filter becomes too large, useful edges may not be extracted. The Sobel filter is based on the following digital derivative:

$$s_x = \{f(x+1, y-1) + 2f(x+1, y) + f(x+1, y+1) - \{f(x-1, y-1) + 2f(x-1, y) + f(x-1, y+1)\} \} \quad (2)$$

$$s_y = \{f(x-1, y+1) + 2f(x, y+1) + f(x+1, y+1) - \{f(x-1, y-1) + 2f(x, y-1) + f(x+1, y-1)\} \} \quad (3)$$

In this paper, the Sobel eight filter operators are utilized to detect the outer-contour of the SCDT wear, as shown in Fig.7a) and a polynomial fitting method, which is as follows, is utilized to obtain the continuous outer-contour, as shown in Fig.7b).

In Fig.8, the real radius of the SCDT is used to calibrate the tool arc in its image. So the Hough arc transform is employed to obtain the tool arc radius and the arc center coordinate in the image coordinate system, shown in Fig.8 and the new image is denoted as $C(x, y)$.

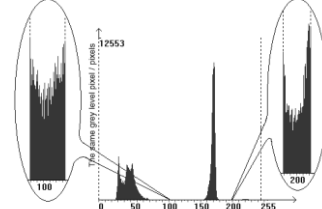


Fig.5 Grey-level histogram of Fig.2a)

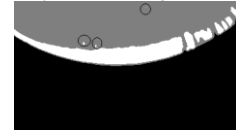


Fig.6 Tri-value image with the feigned wear lands (white)

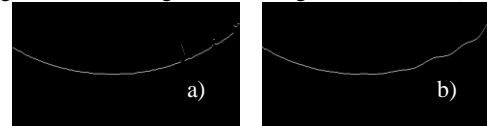


Fig.7 Outer contour of SCDT after the edge detection a) Sobel edge detection and b) Polynomial fitting outer-contour

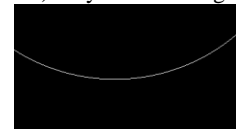


Fig.8 Arc of the tool nose after the Hough arc transform

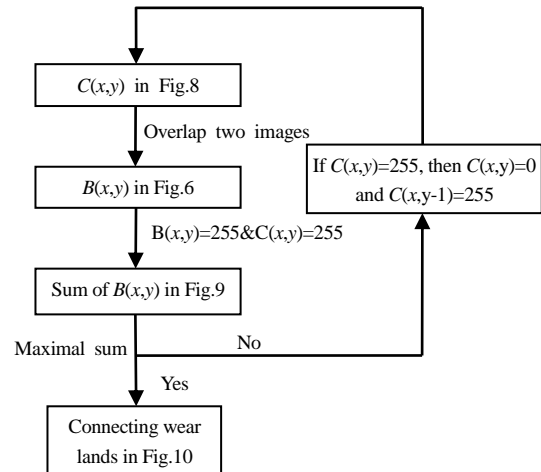


Fig.9 The flow chart of the traverse search method of arc translation

2.2.3 Traverse Search Method of Arc Translation

From the analysis of Fig.2 and 3, the wear land only occurs in and near the outer-contour, so it offers key information that the sum of white pixels along the tool arc increases and then reduces so that the maximal sum which white pixels belong to wear lands can be obtained. Therefore, the traverse search method of arc translation is proposed to eliminate the feigned wear lands (Fig.6) separated from wear and un-wear lands. The elimination of the feigned wear lands is difficult in tool wear study based on digital image processing and is also an extreme key. The flow chart of the traverse search method of arc translation is shown in Fig.9.

The method is that by moving the radius (white pixels in $C(x, y)$)

in Fig.8 which is overlapped with Fig.6, the white pixels of $C(x, y)$ interact with white pixels of the image $B(x, y)$, the sum of those white pixels interacting each other in $B(x, y)$ and $C(x, y)$ is obtained, (Fig.10). When the sum is the largest one, the white pixels are defined as the wear land. If the pixels in $B(x, y)$ are white and neighbor to the wear land, all pixels belong to the wear land. The image is denoted as $D(x, y)$. The new image is denoted as $E(x, y)$, as shown in Fig.11.

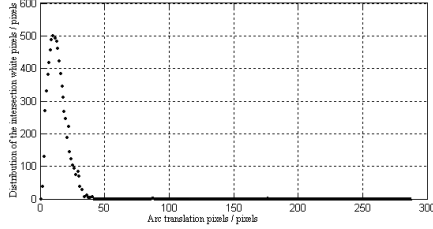


Fig.10 The sum of white pixels intersecting between the arc and the tri-value image with the arc translation method



Fig.11 Tri-value image after eliminating feigned wear lands

2.2.4 Inner-contour Polynomial Fitting Method

Although the traverse search method of arc translation is utilized to eliminate the feigned wear lands in the un-wear land, the feigned wear lands in wear lands which belong to high frequency noises are not eliminated. Due to the effect of light, coolant remains and little relics, which are also high frequency noises, in wear lands do exist discontinuous wear lands and little cuspidal points (Fig.12). The least square polynomial fitting method is employed to filter the high frequency noises in order to eliminate the feigned wear lands in wear lands and to link the discontinuous wear lands.



Fig.12 Discontinuous wear lands and abnormal cusps of the inner-contour

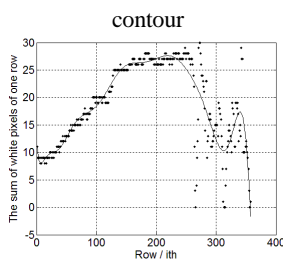


Fig.13 Fitting degree 14 for Fig.12

The inner-contour of the wear lands is continuity, so the least square polynomial fitting is taken advantage to obtain the inner-contour, and (x_i, y_i) ($i=1\sim n$) of the control points are the i^{th} row and the total white pixels of the i^{th} row of the image $E(x, y)$, separately.

The polynomial function is

$$y = f(x) = a_0 + a_1x + \dots + a_mx^m = \sum_{i=0}^m a_i x^i \quad (m < n), \quad (4)$$

where (x_i, y_i) ($i=1\sim n$) are the control point coordinates in one coordinate system, the above function is used for every control point to obtain the linear equation group, where n in the linear equation group are more than $m+1$ (unknown parameters), the value of the unknown parameters by the equation group cannot be gotten, which is called as an over-determined linear equation group. So the least

square polynomial fitting will be used, which is

$$S = \sum_{i=1}^n \Delta_i^2 = \sum_{i=1}^n \left(\sum_{j=1}^m a_j x_i^j - y_i \right)^2. \quad (5)$$

If S is minimal, then these unknown parameters a_i ($i=0, \dots, m$) are based on the partial derivative for a_i ($i=0, \dots, m$)

$$\frac{\partial S}{\partial a_k} = 2 \sum_{i=1}^n \left(\sum_{j=1}^m a_j x_i^j - y_i \right) x_i^k = 0 \quad (k=0, \dots, m). \quad (6)$$

Fig.13 shows the relationship between the sum of white pixels for each row in wear lands and the result after filtering the wear feigned lands by using the least square polynomial fitting method. Then after combining the outline-curve with the least square polynomial fitting result of tool wear lands, the wear land is obtained as shown in Fig.14.



Fig.14 Final wear land

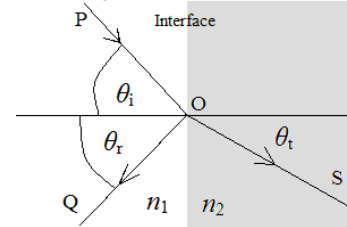


Fig.15 Schematic diagram of relationship between light reflection and refraction

Fig.14 shows that the average wear width of rake face (VB) (AC-line just as shown in Fig.3) is 23.863 pixels and max (VB_{max}) 32 pixels. And according to the image calibration, the calibration value is $0.0576\mu\text{m}$, so the VB is $1.375\mu\text{m}$, VB_{max} is $1.84\mu\text{m}$ and the worn area (AC-land just as shown in Fig.3) is $28.702\mu\text{m}^2$ in the physical scale.

2.3 Auto-regressive Calibration Method

When light moves from a medium of a given refractive index n_1 into a second medium with refractive index n_2 , both reflection and refraction of the light may occur, shown as Fig.15.

In the diagram on the right, the fraction of the incident power that is reflected from the interface is given by the reflection coefficient R . The reflection coefficient R is given by

$$R = \left[\frac{\sin(\theta_i - \theta_t)}{\sin(\theta_i + \theta_t)} \right]^2 + \left[\frac{\tan(\theta_i - \theta_t)}{\tan(\theta_i + \theta_t)} \right]^2 \quad (7)$$

$$= \left[\frac{n_1 \cos(\theta_i) - n_2 \cos(\theta_t)}{n_1 \cos(\theta_i) + n_2 \cos(\theta_t)} \right]^2 + \left[\frac{n_1 \cos(\theta_i) - n_2 \cos(\theta_t)}{n_1 \cos(\theta_i) + n_2 \cos(\theta_t)} \right]^2$$

$$= \left[\frac{n_1 \cos(\theta_i) - n_2 \sqrt{1 - \left(\frac{n_1}{n_2} \sin(\theta_i)\right)^2}}{n_1 \cos(\theta_i) + n_2 \sqrt{1 - \left(\frac{n_1}{n_2} \sin(\theta_i)\right)^2}} \right]^2 + \left[\frac{n_1 \sqrt{1 - \left(\frac{n_1}{n_2} \sin(\theta_i)\right)^2} - n_2 \cos(\theta_i)}{n_1 \sqrt{1 - \left(\frac{n_1}{n_2} \sin(\theta_i)\right)^2} + n_2 \cos(\theta_i)} \right]^2$$

where θ_t can be derived from θ_i by Snell's law and is simplified using trigonometric identities. Fig.16 shows the relation between reflection coefficient and incident angle of single crystal diamond and the curve indicates why the un-wear land is grey and the wear lands is white.

Fig.17 shows the vectors used to define the bidirectional reflectance distribution function (BRDF $f_r(\omega_i, \omega_o)$). All vectors are an unit length. ω_i points toward the light source. ω_o points toward the camera. n is the surface normal. The BRDF was defined by Edward Nicodemus in the mid-sixties. The modern definition is

$$f_r(\omega_i, \omega_o) = \frac{dL_r(\omega_o)}{dE_i(\omega_i)} = \frac{dL_r(\omega_o)}{dL_i(\omega_i) \cos(\theta_i) d\omega_i}, \quad (8)$$

where L is the radiance, E is the irradiance, and θ_i is the angle made between ω_i and the surface normal, n . Because the tool wear is relatively very small and the distance to the camera is relatively extremely long so that the angle θ_i is around zero, the bidirectional reflectance distribution function does not almost affect on the grey level of image.

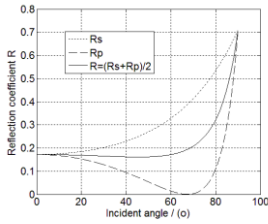


Fig.16 Variables between reflection coefficient and incident angle of single crystal diamond ($n_1=1, n_2=2.4176$)

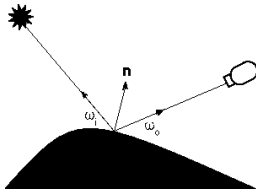


Fig.17 Schematic diagram of the light reflectance distribution

Based on the digital image pre-processing method, the inner- and outer-contours can be obtained. The grey level of the inner-contour of original image is calibrated with zero, and the (i^{th}, j^{th}) grey gradient compared with the un-wear land grey level is the reflection coefficient R_i , so that the incident angle θ_i can be resolved, and then the depth of tool wear is inverse tangent of the incident angle θ_i . The sum of the depth of tool wear for all pixels from the inner-contour to outer-contour is calibrated with the depth of outer-contour (B'B-curve just as shown in Fig.3) which can be calculated with tool parameters, as shown in Tab.1. The calibration method is auto-regressive calibration method. Fig.18 is the result based on auto-regressive calibration method for the 200th Row. And Fig.19a is the 3D topography of tool wear land (BC-land just as shown in Fig.3) based on the new auto-regressive calibration method and VB_{max} is $1.84\mu m$, and Fig.19b is its SEM photograph and VB_{max} is around $2.0\mu m$. So the result shows that the topographic surface of the tool wear lands is extremely similar.

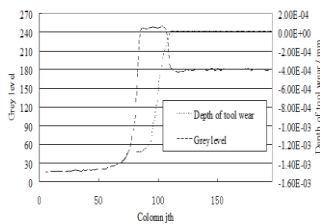


Fig.18 BC-curve of the 200th row of the tool wear image based on the auto-regressive calibration method

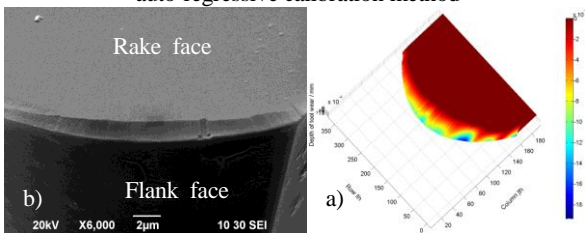


Fig.19 Tool wear land a) 3D reconstruction using the auto-regressive calibration method and b) SEM photograph (View angle 50°)

3. Discussion

3.1 Effect of Thresholds

To estimate the algorithm's reliability, the method is used to detect the wear land for another SCDT, which arc radius is 2.5mm. By using the previous method to process its image with the two thresholds 94 & 184, the result shows in Fig.20.

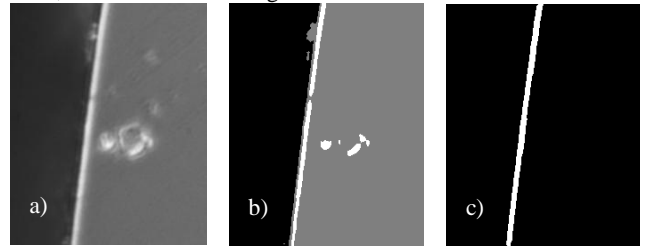


Fig.20 Wear detection of raster milling cutter with radii of 2.5mm (a) Initial image, (b) Tri-value image and (c) Wear land image

When the two thresholds are chosen, the values fluctuate in one certain range due to coolant remains, chip relics and light, the effect of thresholds must be considered. Three different groups of two thresholds are 91 & 180, 94 & 184 and 96 & 187, to segment its initial image to extract tool wear lands, separately and then to calculate sum of white pixels for each row, which result shows in Fig.21. The result suggests that, compared with the three different groups of two thresholds, the error is less than 7.8%, the method is self-adaptive and auto-regressive. It is inferred that the algorithm is sufficiently reliable and efficient to filter the noise and to eliminate the feigned wear lands.

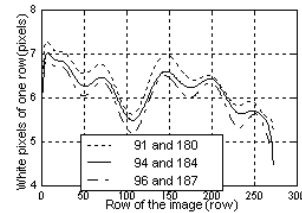


Fig.21 Influence of different thresholds

3.2 Influence of the Polynomial Fitting Degree

Through using the different degrees to fitting the data (Fig.13), the wear area and maximal wear width are shown in Fig.22. From Fig.22a the degree is one in the range between 10 and 20, and from Fig.22b, the degree is more than 13. The optimal degree is 14, because of considering the computer consuming time.

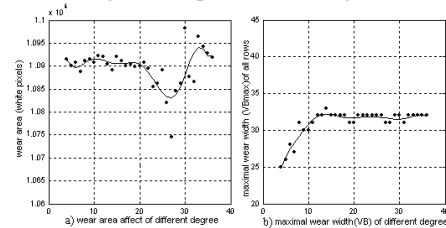


Fig.22 Effects of different fitting degrees on tool wear lands a) wear area effect and b) VB_{max} effect

The result indicates that, in the polynomial fitting, the bigger the degree, the more sensitive it is to high frequency (HF) signals and the greater the computer consuming time. So, when the high frequency signals are filtered, whether the fitting degree is fit or not is the key to the result.

4. Conclusions

In this paper, a new auto-regressive calibration algorithm using a digital image being in-process captured through an in-process measurement system mounted in the UPRM machine 705G is developed to reconstruct 3D topography of the SCDT wear lands. The method is reliable to solve the extreme difficulties from strongly harmful impacts on the image, such as effects of relics of the coolant

and chips and light upon the rake face. Some concluding remarks are given as follows:

- 1) By using the digital image processing technique such as median filtering, threshold segmentation, edge detection and Hough arc transform, the tool wear lands are reliably separated from a tool wear image and the feigned wear lands is eliminated by the traverse search method of arc translation;
- 2) The least square polynomial fitting method is adopted to fit the inner and outer-contour of wear lands, which filters high frequency noises and smoothes the discontinuous wear lands;
- 3) The new auto-regressive calibration method is developed to reconstruct the surface topography of the tool wear, which is extremely similar to its SEM photograph, and the VB_{max} of the wear land is almost equal;
- 4) The wear land can be completely extracted and the tool wear area, maximal tool wear width, average tool wear width and worn volume can be automatically calculated by the new auto-regressive calibration method, which provides one possible solution for the in-process 3d-wear measurement of the SCDT wear;
- 5) The reliability of the algorithm is validated, auto-regressive and self-adaptive.

ACKNOWLEDGEMENT

The authors express their gratitude to The Research Grants Council of Hong Kong Special Administrative Region of the People's Republic of China for providing financial support (Project No. PolyU 5287/10E) and express their sincere thanks to all members of State Key Laboratory in Ultra-precision Machining Technology in The Hong Kong Polytechnic University for their assistance in the experimental work.

REFERENCES

1. C. Everson, S.H. Cheraghi, "The application of acoustic emission for precision drilling process monitoring", *Int. J. Mach. Tools Manuf.*, Vol. 39, No. 3, p.371-387, 1999.
2. H.M. Ertunc, and C.Oysu, "Drill wear monitoring using cutting force signals", *Mechatronice*, Vol. 14, p.533-548, 2004.
3. T.I. El-Wardany, D. Gao and M.A. Elbestawi, "Tool condition monitoring in drilling using vibration signature analysis", *Int. J. Mach. Tools Manuf.*, Vol. 36, No. 6, p.687-711, 1996.
4. S.R. Hayashi, C.E. Thomas and D.G. Wildes, "Tool break detection by monitoring ultrasonic vibrations", *Ann. CIRP*, Vol. 37, No. 1, p.61-64, 1988.
5. O. Tauno and K. Lembit, "Digital Tool Wear Measuring Video System, Estonia", In: Proceedings of 2nd International Conference of DAAAM National Estonia: 2nd Danube-Adria Association for Automation and Metrology conference, Tallinn, p.144 - 146, 2000.
6. S.C. Lin and C.J. Ting, "Tool wear monitoring in drilling using force signals", *Wear*, Vol. 180, No. 1, p.53-60, 1995.
7. F.J. Alonso, D.R. Salgado, "Analysis of the structure of vibration signals for tool wear detection", *Mechanical Systems and Signal Processing*, Vol. 22, p.735-748, 2008.
8. K.V.B.S. Kalyan Kumar and S.K. Choudhury, "Investigation of tool wear and cutting force in cryogenic machining using design of experiments", *Journal of materials processing Technology*, Vol. 203, p.95-101, 2008.
9. T. Pfeifer and L. Wieggers, "Reliable tool wear monitoring by optimized image and illumination control in machine vision", *Measurement*, Vol. 28, p.209-218, 2000.
10. J.U. Jeon, S.W. Kim, "Optical flank wear monitoring of cutting tools by image processing", *Wear*, Vol.127, p.117-207, 1988.
11. M. Lanzetta, "A new flexible high-resolution vision sensor for tool condition monitoring", *J. Mater. Process. Technol.*, Vol.119, p.73-82, 2001.
12. K.B. Pedersen, "Wear measurement of cutting tools by computer vision", *Int. J. Machine Tools Manuf.*, Vol.30, p.131-139, 1990.
13. Min-yang Yang, Oh-dal Kwon, "Crater wear measurement using computer vision and automatic focusing", *J. Mater. Process Technol.*, Vol.58, p.362-367, 1996.
14. S. Kurada, C. Bradley, "A machine vision system for tool wear assessment", *Tribol. Int.*, Vol.30, No.4, p.295-304, 1997.
15. A. Karthil, S. Chandra, B. Ramamoorthy, S. Das, "3D tool wear measurement and visualization using stereo imaging", *Int. J. Machine Tools Manuf.*, Vol.37, No.11, p.1573-1581, 1997.
16. K. Niranjan Prasad, B. Ramamoorthy, "Tool wear evaluation by stereo vision and prediction by artificial neural network", *J. Mater. Process. Technol.*, Vol.112, p.43-52, 2001.
17. W. Grzesik, "Influence of tool wear on surface roughness in hard turning using differently shaped ceramic tools", *Wear*, Vol. 265, p.327-335, 2008.
18. M.Anthony Xavier and M. Adithan, "Determining the influence of cutting fluids on tool wear and surface roughness during turning of AISI 304 austenitic stainless steel", *Jouranal of Materials Processing Technology*, Vol. 209, p.900-909, 2009.
19. F. Giusti, M. Santochi, G. Tantussi, "On-line sensing of flank and crater wear of cutting tools", *Ann. CIRP*, Vol. 36, No. 1, p.41-44, 1987.
20. W. Wang, "Flank wear measurement by successive image analysis", *Computers in Industry*, Vol. 56, p.816-830, 2005.
21. W. H. Wang, "Flank wear measurement by a threshold independent method with sub-pixel accuracy", *Int. J. Mach. Tools Manufact.*, Vol. 46, p.199-207, 2006.
22. Jianwen Hu, Y. Kevin Chou, "Characterizations of cutting tool flank wear-land contact", *Wear*, Vol. 263, p.1454-1458, 2007.
23. Tugrul Ozel, Yigit Karpat, Luis Figueira, J. Paulo Davim, "Modelling of surface finish and tool flank wear in turning of AISI D2 steel with ceramic wiper inserts", *Journal of Materials Processing Technology*, Vol. 189, p.192-198, 2007.